Chapter 2
Print ISBN: 978-81-19039-32-6, eBook ISBN: 978-81-19039-33-3

Tuning the Structural, Microstructural and Optical Properties of ZnO with Different Concentration of Cr Doping

Bikram Keshari Das [a], Tanushree Das [a*] and Dipteerekha Das [a]

DOI: 10.9734/bpi/racms/v6/3951B

ABSTRACT

A systematic study on the structural, microstructural and optical properties of Cr doped ZnO nanoceramics with different milling time and temperature has been reported. The weight percent of Cr in ZnO varies from 1 to 4% and the milling time varied from 2h to 10h. X-ray diffraction (XRD) data reveals that up to 3% of Cr can be doped in to ZnO after 10 hour of milling showing single phase polycrystalline Cr-doped ZnO, but for x = 0.04 few peaks related to Cr_2O_3 was noticed. But after calcination at 900 ºC no additional peak related to Cr_2O_3 was observed for x = 0.04 sample forming single phase. So up to x = 0.04 Cr is below the solubility limit of Cr in ZnO by ball milling. The data is well matched with rietveld refinement of XRD pattern. Particle growth was observed from FESEM micrograph after calcination and sintering. The band gap of 2% of Cr doped ZnO varies from 3.18eV to 3.06eV with milling from 2hr to 10hr again with increasing Cr concentration from x = 0 to x = 0.04 the variation of band gap was from 3.22eV to 3.235eV. Cr doped ZnO shows blue shift with doping concentration and sintering.

Keywords: High energy Ball Milling (HEBM); X-ray Diffraction (XRD); Rietveld refinement; Field Emission Scanning Electron Microscopy (FESEM); Diffuse Reflectance Spectroscopy (DRS).

1. INTRODUCTION

Recently, nanostructured semiconductor metal oxide like ZnO, TiO_2, CuO, CoO etc. are of great interest in the field of research as well as industry [1-5]. Among different semiconductor metal oxide ZnO has the highest nanostructures, both in structures and in properties [6]. ZnO has a band gap of 3.37 eV and binding energy of 60 meV, high transparency, outstanding chemical stability, low cost

[a] Nano Innovation Laboratory, School of IKST, Kalinga Institute of Social Sciences (KISS) Deemed to be University, Bhubaneswar-751024, Odisha, India.
**Corresponding author: Dr. Tanushree Das E-mail: tanushree.das@kiss.ac.in;*

production, excellent electrical and optical properties at normal temperature. Due to these excellent characteristics, it has verities of applications in the field of optoelectronics [7], agriculture [8], photocatalysis [9], antibacterial activity [10], gas sensors [11] and anticancer [12]. However, the structure of ZnO can be modified according to research interest and also for different device fabrication. Band gap energy of ZnO can also be modified by a number of synthesis method and by controlling shape and size [13-17]. By doping different elements into ZnO various properties like electrical, magnetic, and optical can be modified. For suitable application ZnO properties has been tuned by doping various transition metal ions like Ni, Fe, Mn, Cu, Ti, Cr and Co [18-25]. Among these, Cr_2O_3 is the most stable phase under usual conditions. Cr_2O_3 has a number of applications in the field of solar absorber, protective coating layers, catalyst etc. [26]. As the ionic radius of Cr^{3+} ion (0.62 Å) is nearly that of Zn^{2+} ion (0.74 Å), Cr^{3+} can easily substitute for Zn^{2+} in the ZnO lattice [27] and can also modify the properties of ZnO. A number of researchers reported a decrease in band gap of ZnO by Cr doping. Decrease in band gap of ZnO was reported by Prakash chand et al. due to Cr and Fe doping [28]. For the preparation of undoped and doped ZnO nanomaterials different methods have been used like ball milling [29], sol-gel [30], hydrothermal [31], combustion [32], co-precipitation [33], biological methods [34] etc. Among these synthesis techniques, high energy ball milling (HEBM) is the most efficient and simple technique to produce large quantity of nanocrystalline powder. Due to the impact of energy fracturing and rewelding of grains takes place and also lead to formation of different composites and alloys [35]. The characterization of nanostructured solids or nanocrystalline materials comprise the explanation of microstructure in terms of (i) grain size and (ii) lattice defects. Grain size can be determined by analysing Field Emission Scanning Electron Microscopy (FESEM), Transmission Electron Microscopy (TEM). X-ray line broadening is an alternative method to find out grain size [36]. The X-ray, FESEM and TEM methods are used to explain microstructure.

In the present paper we have presented in details about variation of structural, microstructural and optical properties with different milling duration, varying concentration and different temperature of Cr doped ZnO nanoceramics and the possible correlation between them has been investigated.

2. EXPERIMENT

2.1 Materials and synthesis procedure

Cr doped ZnO nanoceramics ($Zn_{1-x}Cr_xO$, x = 0-0.04) have been prepared by High Energy Ball Milling technique (HEBM, PM400Retsch, Germany). High purity ZnO and Cr_2O_3 having 99.9% purity (Sigma-Aldrich) have been used as the raw material. Calculated quantity of ZnO and Cr_2O_3 was taken in tungsten carbide (WC) vials with WC balls maintaining ball to powder weight ratio10:1. The samples were milled for different durations (2, 4, 6, 8 and 10h) with an interruption for 30 min after every one hour of milling to avoid overheating. The milled materials were calcinated at 900 ºC for 2hrs.

2.2 Characterization

Structural characterization of the synthesised materials were performed by XRD using a X-ray diffractometer (D8 Advance, Bruker*)* with Cu K_α radiation with (λ = 1.5406 Å) in the 2θ range of 20º-90º. The Rietveld refinement of the XRD patterns was executed by the "FullProf" program. The analysisof the results were taken place by comparing with standard JCPDS files. Crystal structure supercell model of all synthesized samples were done by using VESTA software.The surface morphologies and chemical composition of the milled powder, the pellet sample after calcinations and after sintering at 1000 $^{\circ}$C was analyzed by using Field Emission Scanning Electron Microscopy and EDX spectroscopy (FESEM, Carl Zeiss NTS Ltd, UK). The particle size distribution was computed by use of ImageJ software. The UV-Vis-DRS absorption spectrum of the samples was carried out by using Lambda 750 UV/Vis/NIR Perkin Elmer spectrophotometer to study the optical properties and estimate the energy band gap.

3. RESULTS AND DISCUSSION

3.1 Structural analysis-XRD

Structural analysis of the mechanically alloyed powders (uncalcined and calcined) has been carried out by XRD.

3.1.1 Impact of milling time

Cr doped ZnO nanoceramics ($Zn_{1-x}Cr_xO$, x=0 - 0.04) has been synthesized by HEBM technique at room temperature for different duration of milling (0, 2, 4, 8, 10h) illustrated in Fig. 1(a, c, e, g and i) and corresponding zoomed in view is shown in Fig. 1(b, d, f, h and j) respectively. The peak shifting of the most intense peak along the plane (101) with different milling time is illustrated in Fig. 2(a-e). The distinct peak of Cr_2O_3 and ZnO were observed for 0h or unmilled samples. The peak related to Cr_2O_3 denoted as Δ Fig. 1 (d, f, h and j) and the peak related to ZnO phase marked as (*) as shown in Fig. 1(c, e, g and i). Few sharp peaks related to Cr_2O_3 are observed at 2θ = 41.38, 50.16 and 54.91º for 0h (unmilled) sample is illustrated in Fig. 1(c, e, g, i). It was noticed that with increase in milling time, the peak related to Cr_2O_3 (marked as Δ) disappeared at 10h of milling for Cr^{3+} concentration x≤0.03 (Fig. 1(d, f, h, j)).

However, at higher concentration i, e x = 0.04 some extra peaks associated to Cr_2O_3 were found at 2θ = 41.38º, 50.16º and 54.91º for 10h ball milled sample (Fig. 1 (j)).This suggests that Cr^{3+} is replaced by Zn^{2+} in the ZnO crystal lattice for x =0.01-0.03 just after ball milling the mixture for 10h but for x = 0.04 peak related of Cr_2O_3 is observed at 10h of milling. However, very tiny peaks at 2θ = 28.63°, 39.48°, 50.84° and 61.59° were observed in all the XRD patterns (Fig. 1 (j)) which are not related to Cr_2O_3.

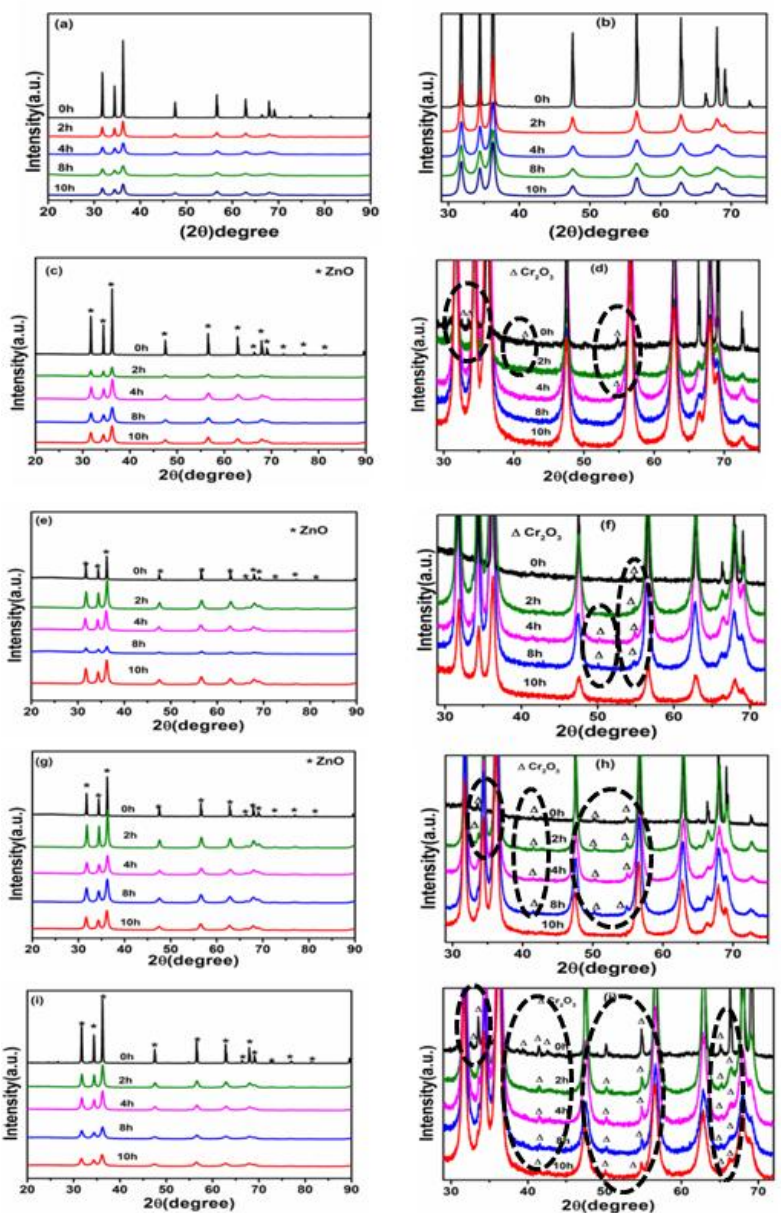

Fig. 1. XRD patterns of $Zn_{1-x}Cr_xO$ nanoceramics as a function of milling time: (a) x = 0, (c) x = 0.01, (e) x = 0.02, (g) x = 0.03, (i) x = 0.04 and the distended view are illustrated in (b), (d), (f), (h) and (j) respectively

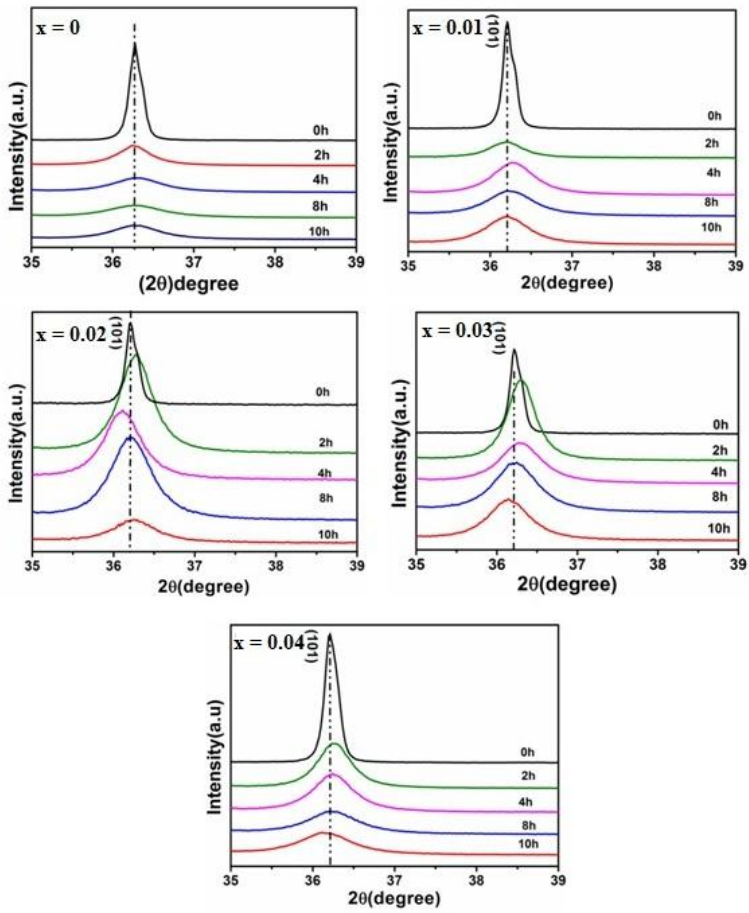

Fig. 2. Shifting of (101) X-ray plane of $Zn_{1-x}Cr_xO$ nanoceramics with milling time

The crystalline nature is clearly shown by the peaks of XRD. The crystal structure of $Zn_{1-x}Cr_xO$ nanoceramic is hexagonal wurtzite structure as observed from the XRD peak and in accordance with JCPDS card no.36-1451 [37-39]. No extra peaks in the XRD pattern was noticed related to Cr or Cr related secondary phases in case of 10h milled sample for $x < 0.04$, this may be owing to the doping of Cr^{+3} ion into the Zn lattice site.Vojisavljevic et al. also reported the similar result [40]. The reduction in peak intensity and enhancement in FWHM of the peak was observed for all samples with increasing milling time. Fig. 2(a-c) shows the shifting of most intense peak (101) for all Cr doped ZnO sample and shifting of peak towards higher 2θ value was observed. This shift is because of the variation in ionic radii of Cr^{3+} and Zn^{2+} which proves that the Cr is effectively

doped into ZnO lattice [41,42]. The strain of the sample was found to be increased after Cr doping. With increase in strain the XRD peak shifting and broadening was noticed for the doped sample [43].

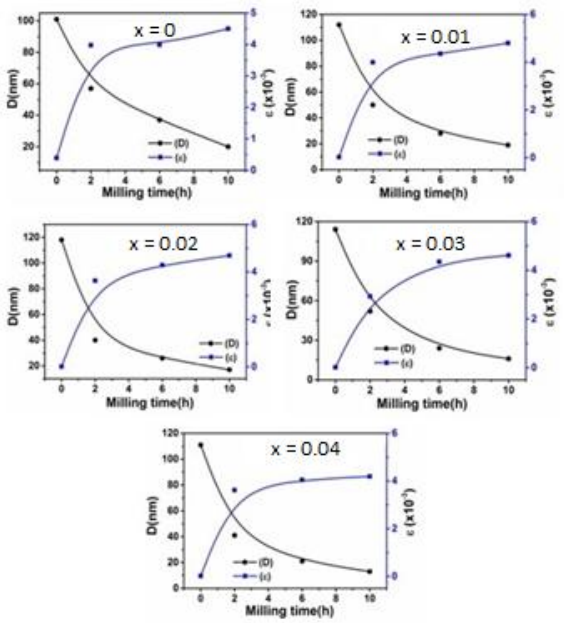

Fig. 3. Variation of crystallite size and strain with different milling time of $Zn_{1-x}Cr_xO$ nanoceramics

3.1.2 Effect of milling time on crystallite size (d) and strain (ε)

Rietveld refinement of the XRD pattern was performed to compute the structural parameters of the milled samples. Williamson-Hall (W-H) method is used to quantify the crystallite size and strain. Fig. 3 represents the variation of crystallite size and strain with different milling duration. As observed from Fig. 3, the crystallite size decreases rapidly for 2h of milling and still decreases slowly with milling up to 10h. The decrease in crystallite size with increase in milling time is because of cracking than rewelding of the mixture during the collision between themselves and with the milling media. The value of lattice strain will be higher when the nanoceramics have more defect concentration [44]. With increase in milling time, lattice imperfection increased which causes increase in lattice strain [45].

The crystallite size systematically reduces with increasing milling time from 0 to 10h however, the strain increases i.e. the crystallite size varies inversely to the lattice strain with milling time. For pure ZnO the crystallite size varies from 101

nm to 20 nm while strain varies from $0.392x10^{-3}$ to $4.5x10^{-3}$. The crystallite size varies from ~ 118 nm to ~ 13 nm while the lattice strain is ranges from 0.0137×10^{-3} to 4.5×10^{-3} for Cr^{3+} doped ZnO respectively. In all samples the strain increases linearly while crystallite size decreases with increasing milling time. This phenomena have been reported by a number of researchers [46–48].

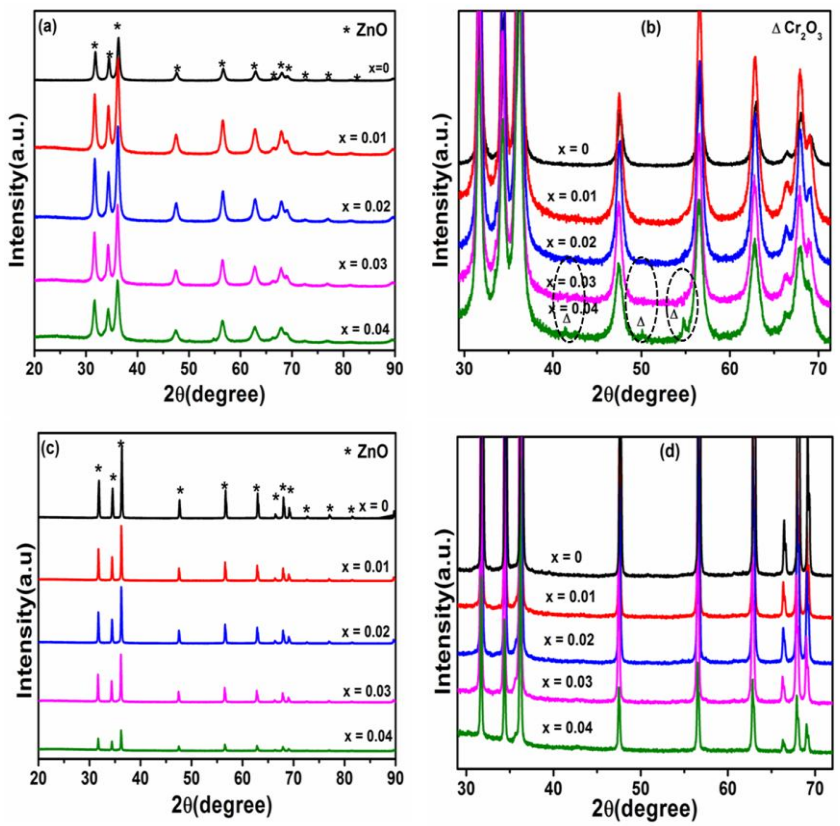

Fig. 4. XRD pattern of Cr doped ZnO nanoceramics: (a) 10h Ball milling, (b) enlarged view of (a), (c) 10h milled followed by calcined at 900 ºC for 2h and (d) enlarged view of (c)

3.1.3 Impact of calcination temperature

Fig. 4(a) illustrates the X-ray diffraction of the 10h ball milled Cr doped ZnO samples with different Cr concentration and Fig. 4(b) shows the enlarged view of Fig. 4(a). The analysis of the XRD patterns shows that the crystal structure of Cr doped ZnO samples is hexagonal.

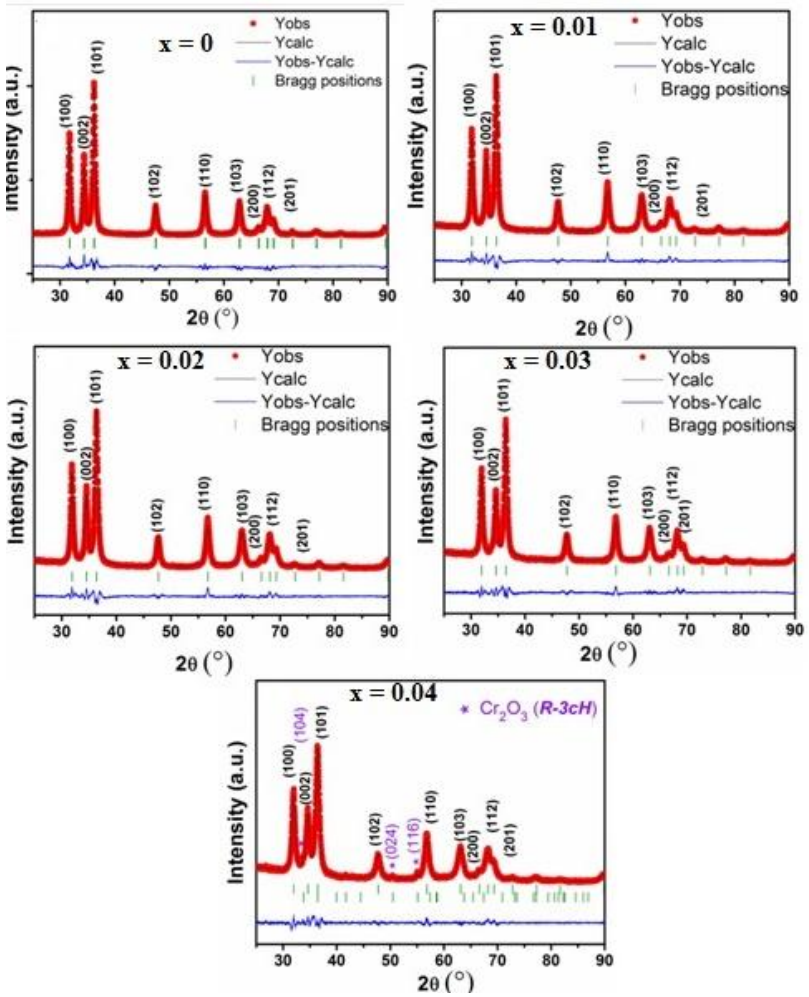

Fig. 5. Rietveld Refinement XRD Profiles of 10h Milled Cr Doped ZnO Sample

The broadening of peak was observed with increase in Cr concentration. The Rietveld refinement of the XRD patterns for these ball milled samples (Fig. 4(a-e) agreed to the experimental result. There is no any impurity or secondary peak related to Cr_2O_3 was observed in the XRD patterns up to x =0.03 for 10h milled samples (Fig. 4 (a) and (b)).

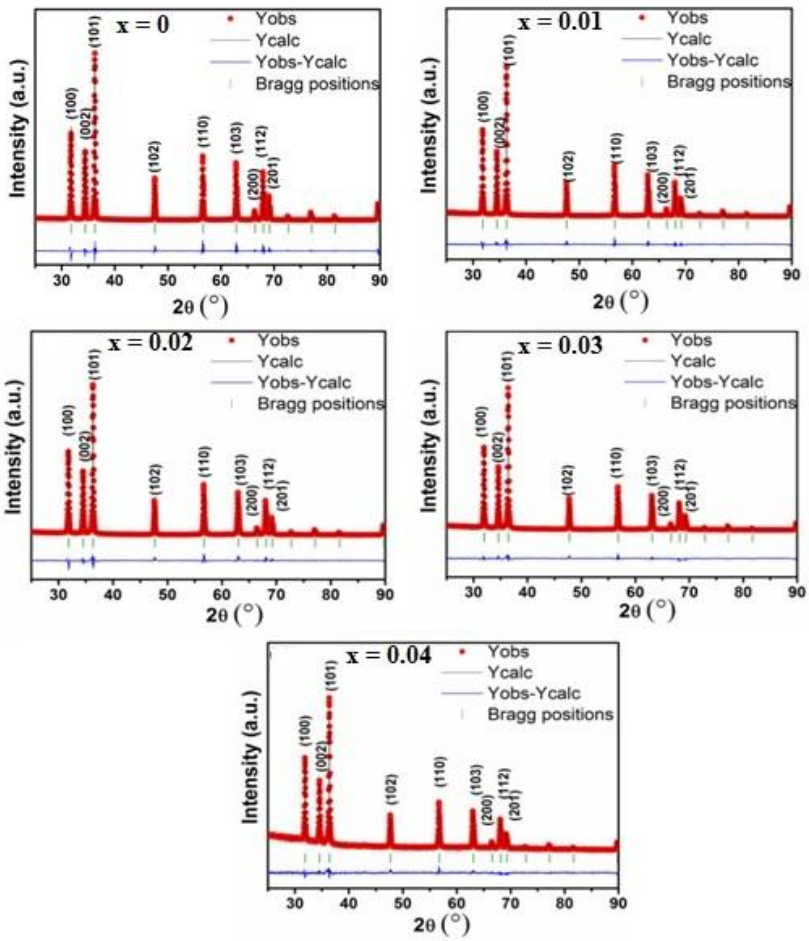

Fig. 6. Rietveld Refinement XRD Patterns of Calcined Cr Doped ZnO Samples

But in case of x = 0.04 some extra peaks associated to Cr_2O_3 are noticed at 2θ = 41.38, 50.16 and 54.91 for x = 0.04 in case of 10h ball milled sample (Fig. 4 (b)), which suggests that Cr^{3+} is replaced by Zn^{2+} in the ZnO crystal lattice for x = 0.01-0.03 just after milling for 10h but for x = 0.04 precipitation of Cr_2O_3 is observed.

The XRD profiles of the milled sample after calcination at 900 ºC for 2 h (Fig. 5(a-e) indicates that the samples with Cr concentration up to 4% (x = 0.04) forms single phase. However very tiny peaks at 2θ = 28.63°, 39.48°, 50.84° and 61.59°

were observed in all the XRD patterns (Fig. 4(c) and (d)). These peaks are not related to Cr_2O_3. Hence, these peaks might be due to any impurity present in the commercial ZnO sample. It indicates that after calcination at 900 ºC the Cr^{3+} ion substitute the Zn^{2+} ion in the crystal lattice of ZnO for the sample with x up to 0.04 giving single phase $Zn_{1-x}Cr_xO$ material and no precipitation of Cr_2O_3 was observed. The Rietveld refinement of XRD profiles of 900 ºC calcined $Zn_{1-x}Cr_xO$ sample was shown in Fig. 6(a-e) and it was good in agreement with observed result. Therefore, we believe that up to 4% of Cr (x=0.04) doping is well below the solubility limit of Cr ion in ZnO lattice by HEBM. More than 4% of Cr doping in ZnO was reported by sol gel method and by a number of researchers [49,50]. Kerista Sebayang et al. reported more than 3.5% of Cr doping by solid state reaction [51]. It is also noticed that upon calcination the peak intensity increased and FWHM decreased which indicates the crystallinity of the $Zn_{1-x}Cr_xO$ sample increased after calcinations [45].

3.1.4 Impact of calcination temperature on structural parameters

The structural parameters of the XRD patterns of 10h ball milled $Zn_{1-x}Cr_xO$ nanoceramics were shown in ((Fig. 7(a-f)) and after calcination at 900 ºC were presented in ((Fig. 8(a-f)). It has been observed from Fig. 7(a) there is no significant modification in the value of lattice parameter (***a*** and ***c***) due to Cr doping. However, a slight increase in the value of both ***a*** and ***c*** was observed after Cr doping which can be due to the lattice distortion caused by doping. But it decreases with increases in Cr concentration and this result is consistent with the reported observation [50,52,53]. However after calcination the value of ***a*** and ***c*** is found to decrease (Fig. 8(a)). The ***c/a*** ratio of ZnO is not much increased by Cr doping while the volume of unit cell reduces slowly with increase in Cr concentration (Fig. 7(b)). But after calcination, the tetragonality factor and unit cell volume decreases with increasing in Cr concentration (Fig. 8(b)). The value of *c/a* =1.60 indicates that the hexagonal structure of pure ZnO is not disturbed by Cr substitution or calcination. The volume of the unit cell was computed by using the equation.

$$V = 0.886 \times a^2 \times c \quad (1)$$

The change in lattice parameter, volume and *c/a* ratio due to calcination may be attributed to change in particle size and quantum size effect [54]. The crystallite size (D) was calculated by Scherer equation and W-H method is used to calculate the strain (**ε)** induced in the sample.The change of crystallite size and strain with increase in Cr concentration were given in Fig. 7(c). It was found that the crystallite size decreases with increases in Cr concentration in ZnO. Which may be caused by doping of Cr atom in the ZnO lattice [55].

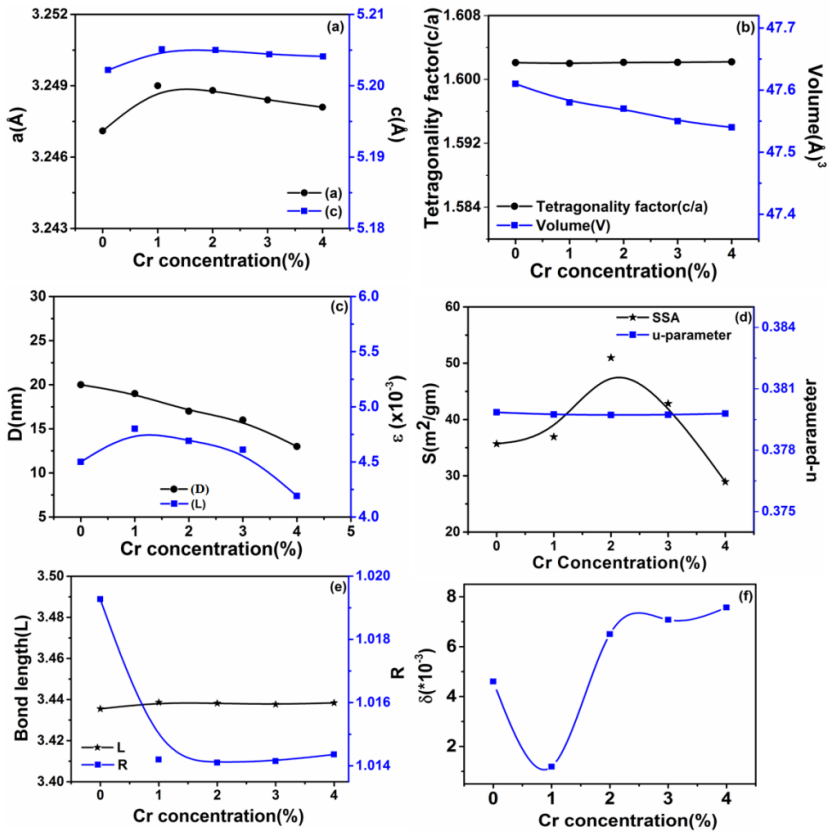

Fig. 7. Variation of structural parameter with Cr concentration of 10h milled Cr doped ZnO samples (a) Latice pameter 'a' and 'c',(b) c/a ratio and V, (c) D and ε, (d) SSA and u-parameter (e) L and R and (f) dislocation density(δ)

The reduction in size may be because of lattice distortion of the ZnO crystal structure due to doping of smaller size Cr into ZnO lattice [55]. Similar result was also reported by a number of researchers [53,56]. The lattice strain is increased after Cr doping but with increase in Cr concentration it is found to be decreased. The result is quite similar as observed by Santi Septiani et al. [52]. After calcination crystallite size of all sample increases significantly which might be due to the recrystallization of $Zn_{1-x}Cr_xO$ nanoceramics [54]. In addition with increase in crystallite size lattice strain was reduced. This can be due to decrease of defect concentration in ZnO and structural relaxation [45] Fig. 8(c). Another reason for the reduction of lattice strain with calcination is due to improved crystallinity with temperature. Fig. 7(d) shows the change of specific surface area and u-parameter with Cr concentration.

The specific surface area (SSA) of sample was computed by using the relation

$$S = \frac{6\times10^3}{D_p\times\rho} \quad (2)$$

The specific surface area of Cr doped ZnO shows larger value up to 2% of Cr doping than pure ZnO which is slightly decreases for 3% and 4% of doping. This large value of specific surface area shows the higher reactivity of sample [57]. The specific surface area decreases drastically after calcination which may be due to enhance in crystallite size (Fig. 8(d)).

The u-parameter was calculated by using the formula [41].

$$\mathrm{u} = \frac{1}{3}\left(\frac{a^2}{c^2}\right) + \frac{1}{4} \quad (3)$$

Slight increase in the value of u-parameter was also observed (Fig. 8(d)). The doping induced effect on Zn-O bond length was calculated using relation

$$L = \sqrt{\frac{a^3}{3} + \left(\frac{1}{2} - u\right)^2 c^2} \quad (4)$$

The effect of Cr doping on the variation of Zn-O bond length was shown in Fig. 7(e), which shows a very small variation of bond length with rise in Cr concentration which confirms replacement of ion [58]. The lattice distortion in the crystal structure is due to the change in bond length. The lattice distortion degree was calculated by using the relation

$$\mathrm{R}=\frac{2a(\frac{2}{3})^{1/2}}{c} \quad (5)$$

Small decrease in bond length(L) and lattice distortion(R) was observed after calcination (Fig. 8(e)). In our case, the lattice parameter (***a*** and ***c***) and Zn-O bond length was found to be decreased with increasing the Cr concentration, which confirms the reduction of crystallite size along with unit cell volume and relevant modification in micro strain .

The average value of dislocation density (δ) was calculated by using the relation

$$\delta = \frac{15\beta cos\theta}{4aD} \quad (6)$$

The value of dislocation density (δ) was calculated by taking first three major planes (100), (002), (101) and are shown in Fig. 7(f). It was observed that the value of dislocation density (δ) for x=0.01 doped ZnO is lower than pure ZnO which increases with increase in Cr concentration. The highest value of dislocation density was observed for x = 0.04, indicates the highest hardness among all the samples [59]. In comparison to uncalcined sample, the calcined sample shows lower value of dislocation density Fig. 8(f).

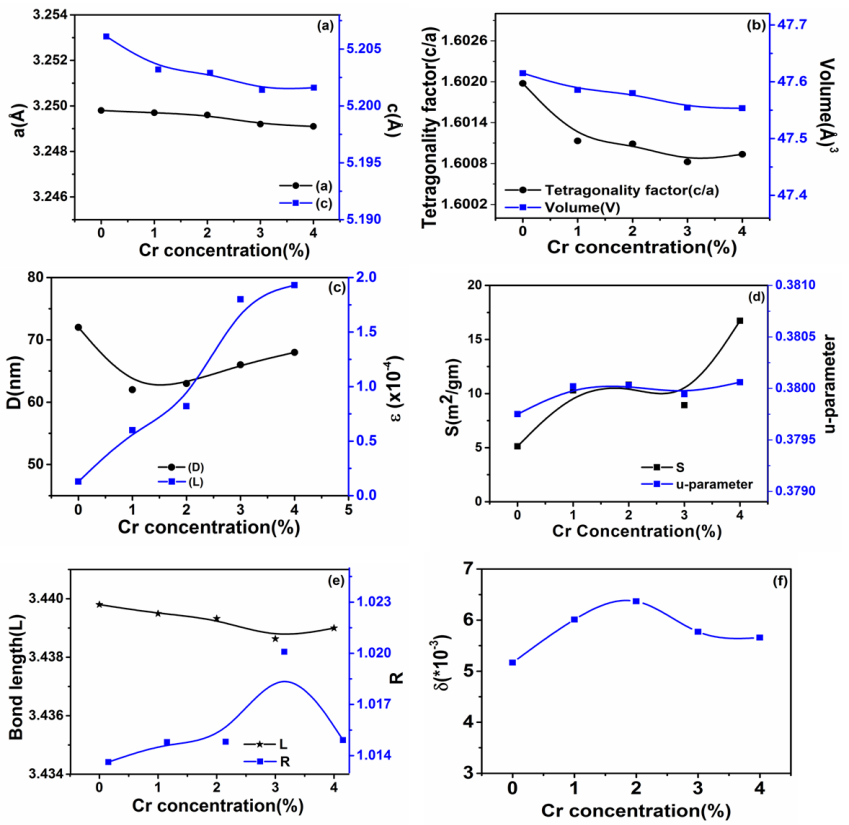

Fig. 8. Variation of structural parameter with Cr concentration of 10h milled and calcined Cr doped ZnO samples (a) Latice pameter 'a' and 'c',(b) c/a ratio and V, (c) D and ε, (d) Specific surface area and u-parameter (e) L and R and (f) dislocation density(δ)

3.1.5 Crystal structure supercell model

To facilitate the actual dopant variation we used periodic 3x3x3 supercell of Cr doped ZnO sample, those are drawn from XRD information and appeared in Fig. 9(a-e).

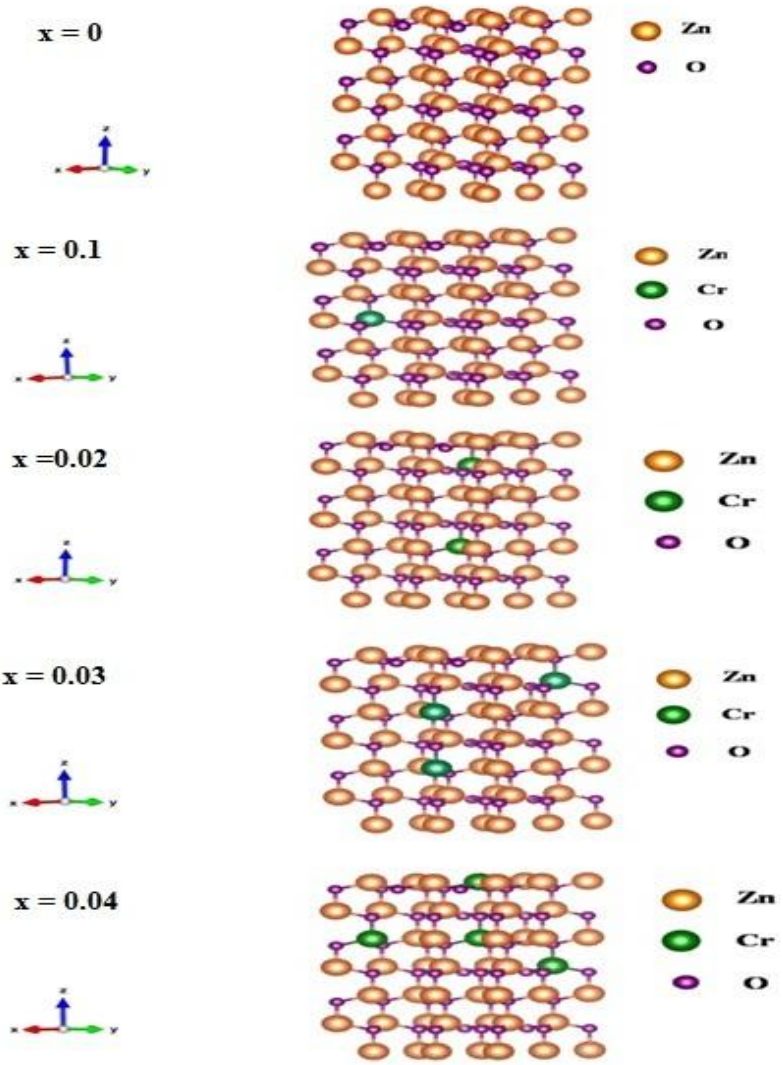

Fig. 9. Wurtzite supercell model of 10h milled powder of $Zn_{1-x}Cr_xO$

The ideal ZnO has a hexagonal wurtzite structure. Fig. 9 (a) represents the supercell of the wurtzite ZnO with total 102 atoms having 51 atoms of zinc and 51 atoms of oxygen. By replacing one, two, three and four zinc by three chromium atoms 1%, 2%, 3% and 4% Cr-doped ZnO samples are obtained. For this situation the super cell contains 50, 49, 48 and 47 atoms of zinc with 1, 2, 3

and 4 atom of chromium for 1%, 2%, 3% and 4% Cr-doped sample respectively along with 51 atoms of oxygen [60].

3.2 Microstructural Analysis

The microstructural analysis of the synthesized samples has been carried out by Field Emission Scanning Electron Microscopy (FESEM).

3.2.1 FESEM analysis

The surface morphological properties of Cr doped ZnO nanoceramics was investigated by FESEM and were shown in Fig. 10 (a, b and c). The morphology of undoped and Cr doped samples is spherical. Due to aggregate of particle some bigger particle of different shape and size are found. Densification of sample also observed after calcination at 900 ºC and sintering at 1000 ºC, before sintering the density of pellet ≤ 77%, whereas after sintering density was found to be ~97% .The average particle size of ball milled Cr doped ZnO sample was found to be in the range of ~ 30 nm (Fig. 11(a). However the particle size after calcination increased and was ranging from 99 nm -204 nm (Fig. 11(b). Again the particle size was found to increase after sintering ranging from174 nm to 938 nm (Fig.11(c). Similar results were observed by R.O. Yathisha et al. [61]. K. Vijayalakshmi also reported that the particle size of ZnO decreases after Cr doping [62]. Compared to that of doped ZnO the particle size of ZnO is much larger.

3.2.2 Energy Dispersive X-Ray (EDX) analysis

The chemical composition of the synthesized materials ($Zn_{1-x}Cr_xO$) were analyzed by EDX and shown in Fig. 12. The EDX spectra of pure ZnO contain only Zn, O and along with the presence of Cr in the Cr doped ZnO samples (Fig. 12). This confirms that Cr is successfully doped into the ZnO host lattice. This is well supported by the XRD result. No impurities were noticed in the sample which validates purity of the samples.

3.3 Optical Analysis

Diffuse Reflectance Spectroscopy (DRS) was used to study the optical behaviour of synthesized nanoceramics samples. All spectra were recorded at room temperature in the wave length range of 300-800nm. Here it is executed to see the effect of dopant on the energy band gap of ZnO was observed.

3.3.1 Determination of band gap energy (E_g)

Kubelka-Munk method was used to calculate the band gap energy (E_g) of both doped and undoped samples [63,64] by plotting the $F(R)^2$ Vs hv and extrapolating the linear part of the curve to $F(R)^2=0$.

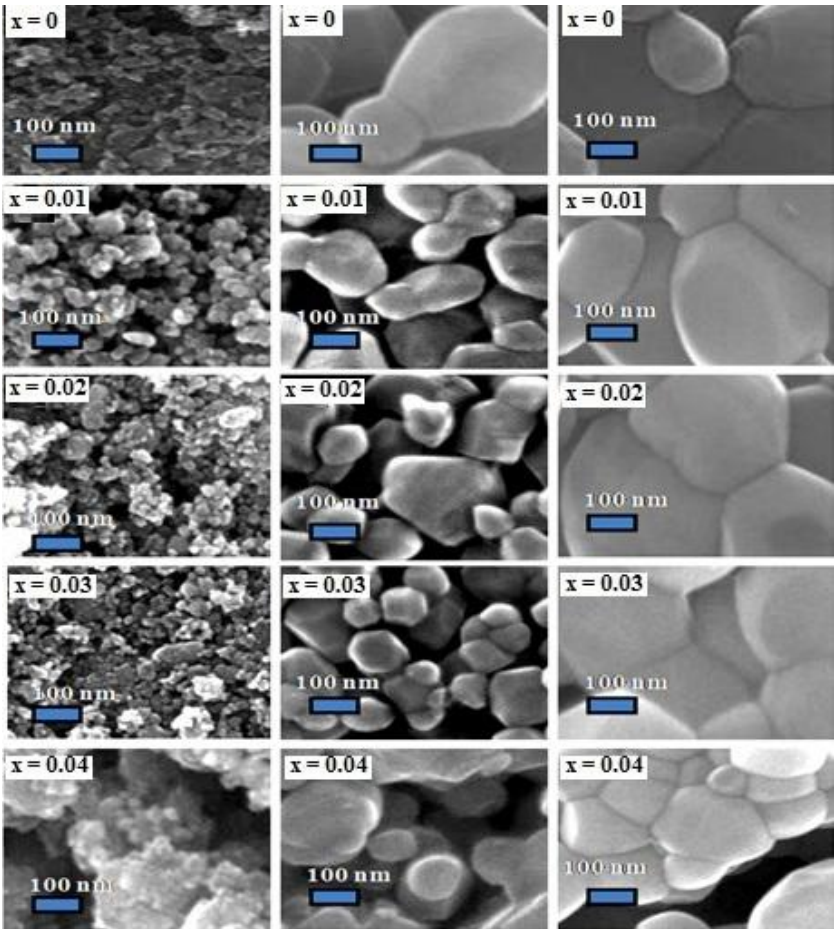

Fig. 10. FESEM micrograph of $Zn_{1-x}Cr_xO$(x = 0 - 0.04) nanoceramics: (a) 10h milled uncalcined powder,(b) unsintered pellet of 10h milled calcined (900 ºC) pellet and (c) sintered(1000 ºC) pellet of calcined powder

3.3.2 Variation of band gap energy (E_g) with milling time

The reflectance spectra of 2% Cr doped ZnO was examined with different duration of milling and shown in Fig. 13.

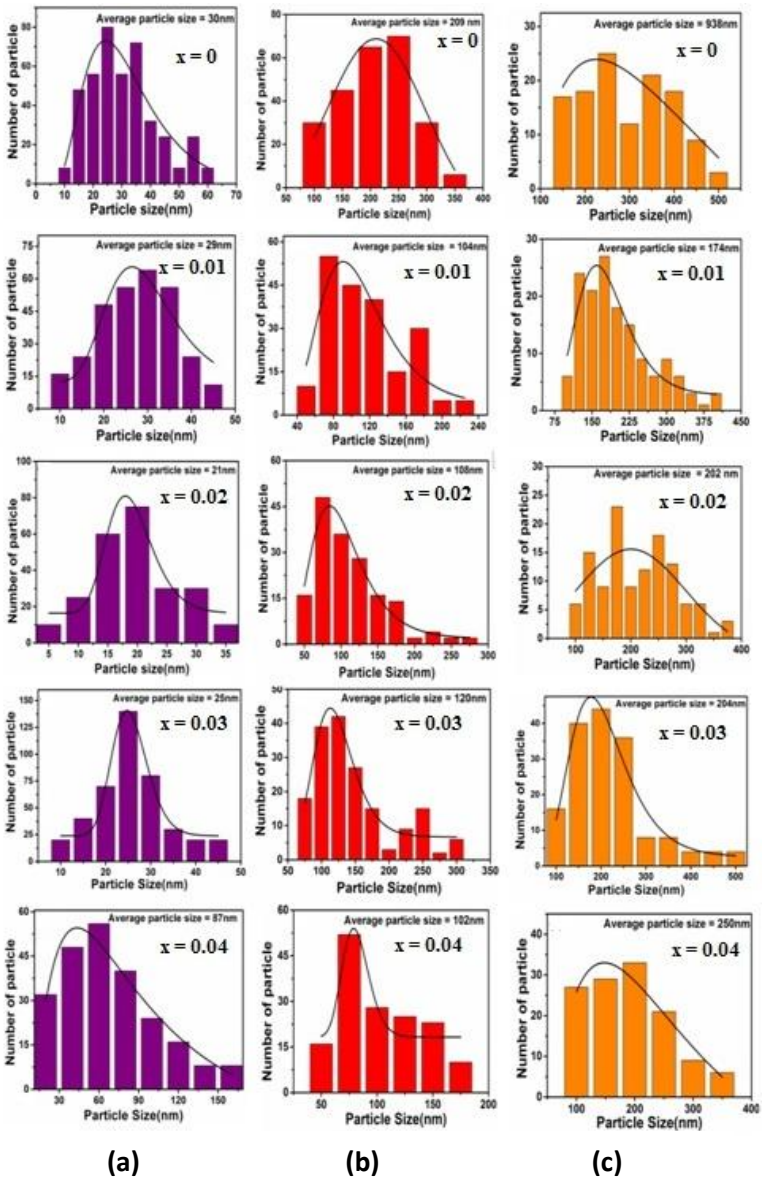

Fig. 11. Particle size distribution of $Zn_{1-x}Cr_xO$ samples (a) 10h milled uncalcined powder, (b) Pellet of 10h ball milled powder and calcination at 900ºC and (c) sintered (1000 ºC) pellet of calcined powder

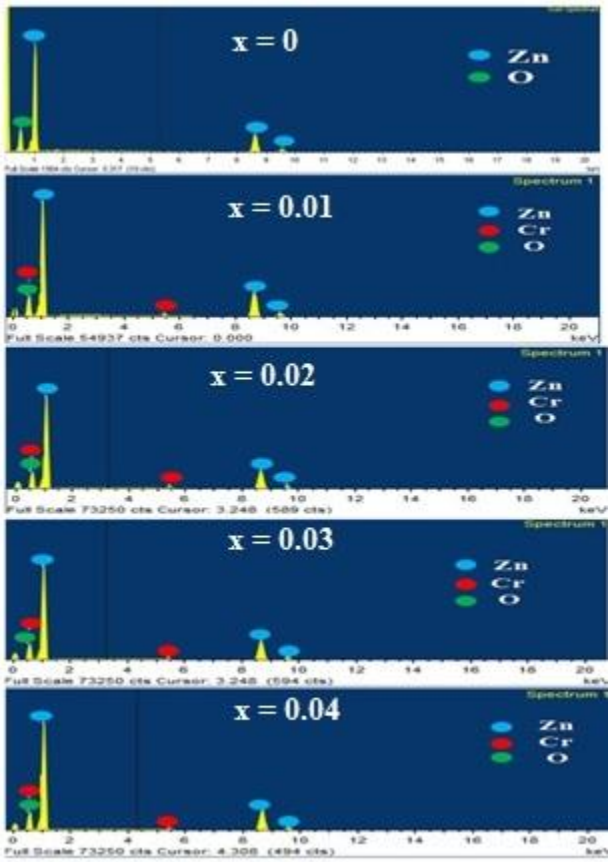

Fig. 12. EDX spectra of $Zn_{1-x}Cr_xO$ nanoceramics

The calculated band gap for these samples is depicted in Fig. 14. The band gap was observed to reduce monotonically with increase in milling time from 3.18eV to 3.06eV.Our observation is further supported by the earlier observation [65].

3.3.3 Band gap energy (E_g) variation with Cr concentration

The DRS plot of calcined 10h milled Cr doped ZnO samples are shown in Fig. 15 and the variation of corresponding band gap energy was show in Fig. 16. The calculated band gap for Cr doped ZnO samples were found to increase with rising Cr concentration (blue shift). Over all a very minute variation in the band gap was observed. In our system, the variation of E_g may be due to the presence of strain inside the crystal supported by XRD analysis. The origin of strain as a result of the presence of lattice defects (dislocation, point), bond length variation, bond angle etc [66,67] due to ball milling.

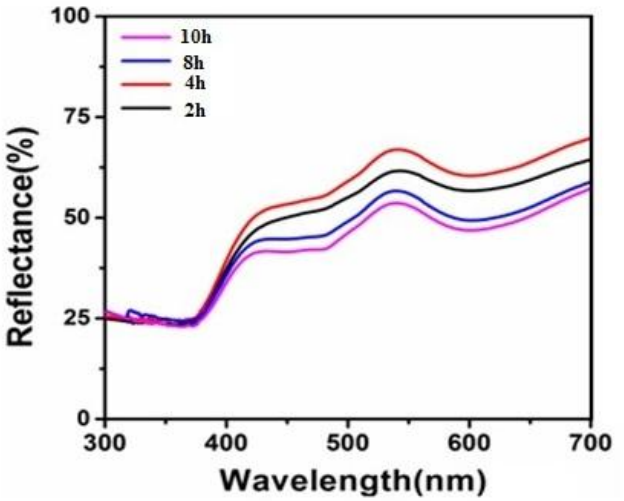

Fig. 13. DRS spectra of 2% Cr doped ZnO powder sample with milling time

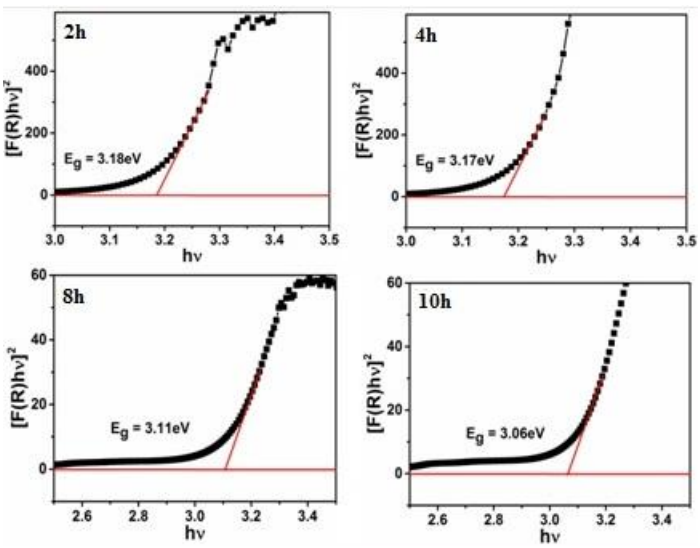

Fig. 14. Variation of energy band gap of 2% Cr doped ZnO sample with milling time

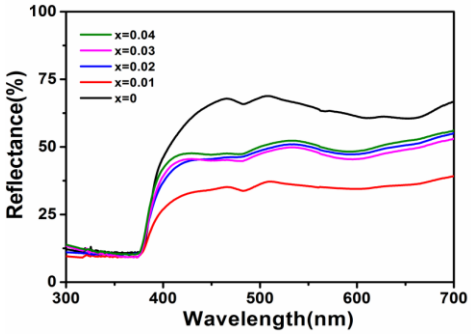

Fig. 15. DRS spectra of 10h milled $Zn_{1-x}Cr_xO$ nanoceramics after calcination

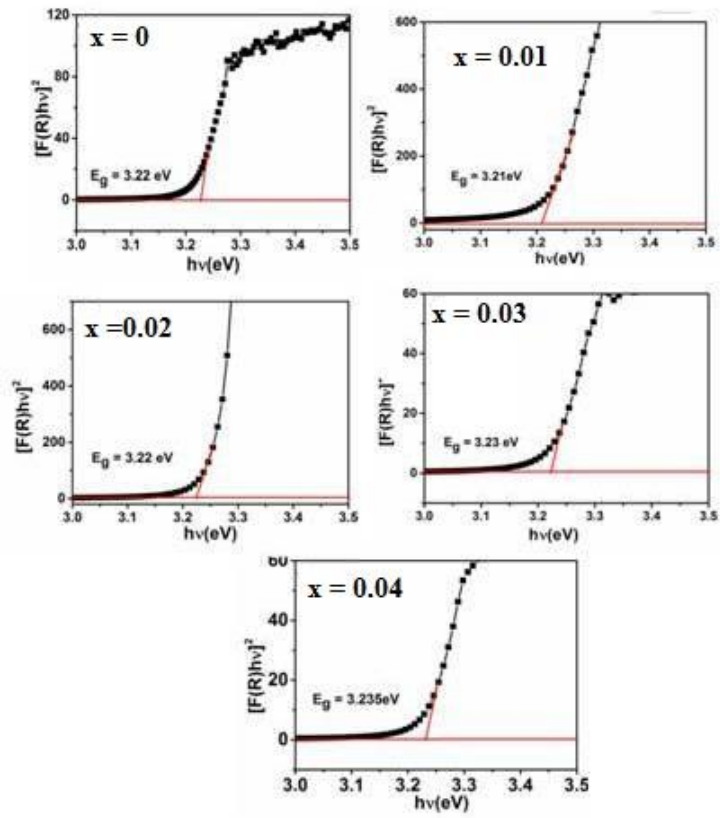

Fig. 16. Variation of band gap energy of $Zn_{1-x}Cr_xO$ nanoceramics

The variation of the lattice parameter is also a possible reason for the change of E_g. Additionally change in structural parameter, grain size, lattice strain etc. are the factors responsible for the change of band gap [68]. This result shows the band gap tuning through doping.This suggests possible applications for electronic, optoelectronic and photocatalytic devices. Similar results were reported in literature for Sn doped ZnO [69], Cu doped ZnO [70], Nd doped ZnO thin films [71].

4. CONCLUSION

Cr doped ZnO ($Zn_{1-x}Cr_xO$) nanoceramics with different doping concentration were synthesized successfully using high energy ball milling. Rietveld refinement XRD study showed the hexagonal wurtzite structure of synthesized nanoceramics and did not induce impurity phase. The increase of lattice constants, strain, bond length, u-parameter, change in c/a ratio, volume, reduction of average crystallite size and the change in band gap energy shows that Cr has really doped into ZnO lattice. The crystallite size decreases whereas strain increases linearly with increase in duration of milling. After calcination at 900˚C the impurity phase of Cr_2O_3 disappeared. The crystallite size decreased after Cr doping whereas strain increased. Calcined sample have bigger crystallite size and less strain than uncalcined. After calcination the specific surface area was found to decrease. The growth of particle was observed after calcination and sintering. The band gap energy found to be reduced with increase in milling time but found to be increased with increase in Cr concentration shows a blue shift showing the suitability of the sample for optoelectronic device applications.

ACKNOWLEDGEMENT

The authors would like to thank the Science and Engineering Research Board (SERB), Govt. of India for providing financial support to carry out the research work of this paper for the project CRG/2019/003315.

Authors are also thankful to Dr. S.K.S. Parashar, Dr. Kajal Parashar of KIIT University, Bhubaneswar for providing facilities to synthesize the sample and Dr. Balaram Sahoo of IISc. Bangalore for helping in material characterization.

COMPETING INTERESTS

Authors have declared that no competing interests exist.

REFERENCES

1. Akgu FA. Influence of Ti doping on ZnO nanocomposites: Synthesis and structural characterization. Composites Part B. 2016;91:589-594.
2. Diebold U. The surface science of titanium dioxide. Surf. Sci. Rep. 2003;48: 53-229.

3. Akimoto K, Ishizuka S, Yanagita M, Nawa Y, Paul GK, Sakurai T. Thin film deposition of Cu_2O and application for solar cells. Sol Energy. 2006;80: 715-722.
4. Gao F, Liu XJ, Zhang JS, Song MZ, Li N. Photovoltaic properties of the p-CuO/n-Si hetero junction prepared through reactive magnetron sputtering, J ApplPhys. 2012;111: 084507-11.
5. Yuhas BD, Yang P. Nanowire-based all-oxide solar cells. J Am Chem Soc. 2009;131: 3756-61.
6. Reddya IN, Ch. V. Reddya, Sreedharb M, Shima J, Choc M, Kim D. Effect of ball milling on optical properties and visible photocatalytic activity of Fe doped ZnO nanoparticles. Mater. Sci. Eng. B. 2019;240:33–40.
7. Yuan Z, Fu M, Ren Y. Optoelectronic properties of ZnO nanoparticles / pentacene heterojunction photodiode. J. Electron. Mater. 2014;43: 3270–3275.
8. Nithiya P, Chakra CHS, Ashok CH. Synthesis of TiO_2 and ZnO nanoparticles by facilepolyol method for the assessment of possible agents for seed germination. Mater. Today-Proc. 2015;2: 4483–4488.
9. Wang Y, Zhao X, Duan L, Wang F, Niu H, Guo W, Ali A. Structure, luminescence and photocatalytic activity of Mg-doped ZnO nanoparticles prepared by auto combustion method. Mater. Sci. Semicond. Process. 2015; 29:372–379.
10. Pandimurugan R, Thambidurai S. UV protection and antibacterial properties of seaweed capped ZnO nanoparticles coated cotton fabrics. Int. J. Biol. Macromol. 2017; 105:788–795.
11. Kazemi AS, Afzalzadeh R, Abadyan M. ZnO nanoparticles as ethanol gas sensors and the effective parameters on their performance. J. Mater. Sci. Technol. 2013; 29:393–400.
12. Sisubalan N, Ramkumar VS, Pugazhendhi A, Karthikeyan C, Indira K, Gopinath K, Hameed ASH, Basha MHG. ROS-mediated cytotoxic activity of ZnO and CeO_2 nanoparticles synthesized using the Rubiacordifolia L. leaf extract on MG-63 human osteosarcoma cell lines. Environ. Sci. Pollut. Res. 2017; 25:10482–10492.
13. Gulera A, Ardab L, Doganc N, Boyrazd C, Ozugurlue E. The annealing effect on microstructure and ESR properties of (Cu/Ni) codoped ZnO nanoparticles. Ceram. Int. 2019; 45:1737–1745.
14. Heiba ZK, Arda L, Mohammed MB, Nasser YM, Dogan N. Effect of annealing temperature on structural and magnetic properties of $Zn_{0.94}Co_{0.05}Cu_{0.01}O$. J. Supercond. Nov. Magn. 2013; 26:3487.
15. Choi Y, Kang J, Hwang D, Park S. Electron devices, recent advances in ZnO-based light-emitting diodes. IEEE Trans. Electron Devices. 2010; 57: 26.
16. Tosun M, Ataoglu S, Arda L, Ozturk O, Asikuzun E, Akcan D, Cakiroglu O. Structural and mechanical properties of Zn-CuO nanoparticles. Mater.Sci. Eng. 2014; A590:416–422.
17. Salem JK, Hammad TM. The effect of surfactants on the particle size and optical properties of precipitated ZnO nanoparticles. J. Mater. Sci. Eng. 2009; 3:38.

18. Aleksandra BD, Chen XY, Leung YH. Nickel-zinc mixed metal oxide: co precipitation synthesis and application as gas sensors. Mater. Chem. 2012; 22:6526–6535.
19. Hsu HP, Lin DY, Lu CY, Ko TS, Chen HZ. Effect of lithium doping on microstructural and optical properties of ZnO nanocrystalline films prepared by the sol-gel method. Crystals. 2018; 8:228.
20. Gürbüz O, Okutan M. Structural, electrical, and dielectric properties of Cr doped ZnO thin films: Role of Cr concentration. Appl. Surf. Sci. 2016; 387: 1211-8.
21. Mao Y, Ma S, Li X, Wang C, Li F, Yang X, Zhu J, Ma L. Effect of Mn doping on the microstructures and sensing properties of ZnO nanofibers. Appl. Surf. Sci. 2014; 298: 109-15.
22. Das BK, Verma SK, Das T, Panda PK, Parashar K, Suar M, Parashar SKS. Altered electrical properties with controlled copper doping in ZnO nanoparticles by ROS induction and apoptosis. Chem. Bio. Inter. 2019; 297:141–154.
23. Das BK, Das T, Parashar K, Parashar SKS. Structural, bandgap tuning and electrical properties of Cu doped ZnO nanoparticles synthesized by mechanical alloying. J. Mater. Sci. Mater. Electron. 2017; 28:15127–15134.
24. Das B K, Das T, Parashar K, Parashar SKS. Structural, optical and dielectric study of Cu doped ZnO nanoparticles synthesised by high energy ball milling. Int. J. Nano Biomater.2017;07:40-49
25. Das T, Das BK, Parashar K, Kumar R, Choudhary HK, Anupama AV, Sahoo B, Kumar Sahoo P, Parashar SKS. Effect of Sr-doping on sinterability, morphology, structure, photocatalytic activity and AC conductivity of ZnO ceramics. J. Mater. Sci. Mater. Electron. 2017; 28: 13587–13595.
26. Yathishaa RO, Arthoba Nayakaa Y, Vidyasagar CC. Microwave combustion synthesis of hexagonal prism shaped ZnO nanoparticles and effect of Cr on structural, optical and electrical properties of ZnO nanoparticles. Mater. Chem. Phys. 2016; 181:167-175.
27. Zhangn GH, Deng XY, Wang PY, Wang XL, Chen Y, Ma HL, Gengzang DJ. Morphology controlled syntheses of Cr doped ZnO single-crystal nanorods for acetone gas sensor. Mater. Lett. 2016; 165:83–86.
28. Chand P, Gaur A, Kumar A. Effect of Cr and Fe doping on the structural and optical properties of ZnO nanostructures.Int. J. Chem. Nucl. Mater. Metall. Eng. 2014; 8:1229-1232.
29. Shen J, Jiang S, Xu Y, Li M, Zhu S, Chen Z, Lin X, Liu H, Li H, Zhang G. Boron and sodium co-doped ZnO varistor with high stability of pulse current surge, J. Alloys Compd. 2017;728:368–375.
30. Kim HT, Lee SY, Park C. Controls of surface morphology on sol-gel derived ZnO films under isothermal treatment conditions. Vacuum. 2017; 143:312–315.
31. Lv X, Du Y, Li Z, Chen Z, Yang K, Liu T, Zhu C, Du M, Feng Y. High photocatalytic property and crystal growth of spindle-like ZnO microparticles synthesized by one-step hydrothermal method. Vacuum. 2017; 144:229–236.

32. Wang Y, Zhao X, Duan L, Wang F, Niu H, Guo W, Ali A. Structure, luminescence and photocatalytic activity of Mg-doped ZnO nanoparticles prepared by auto combustion method, Mater. Sci. Semicond. Process. 2015; 29:372–379.
33. Goel S, Sinha N, Yadav H, Joseph AJ, Kumar B. Experimental investigation on the structural, dielectric, ferroelectric and piezoelectric properties of La doped ZnO nanoparticles and their application in dye-sensitized solar cells, Phys. E Low-Dimensional Syst. Nanostructures. 2017; 91:72–81.
34. Umaralikhan L, Jaffar MJM. Green synthesis of ZnO and Mg doped ZnO nanoparticles, and its optical properties. J. Mater. Sci. Mater. Electron. 2017; 28:7677–7685.
35. Das BK, Tanushree Das, Parashar K, Parashar SKS, Kumar R, Choudhary HK, Khopkar VB, Anupama AV, Sahoo B. Investigation of structural, morphological and NTCR behaviour of Cu-doped ZnO nanoceramics synthesized by high energy ball milling. Mate. Chem. Phy. 2019; 221:419–429.
36. Ungar T. Characteization of nanocrystalline materials by X-ray line profile analysi. J Mater Sci. 2007; 42:1584–1593.
37. Yilmaz S, Parlak M, Ozcan S, Altunba M, McGlynn E, Bacaksiz E. Structural, optical and magnetic properties of Cr doped ZnO microrods prepared by spray pyrolysis method. Appl. Surf. Sci. 2011;257:9293–9298.
38. Liu Y, Yang Y, Yang J, Guan Q, Liu H, Yang L, Zhang Y, Wang Y, Wei M, Liu L, Fei X. Cheng. Intrinsic ferromagnetic properties in Cr-doped ZnO diluted magnetic semiconductors. J. Solid State Chem. 2011;184:1273–1278.
39. Kumar B, Sinha N, Ray G, Godara S, Gupta MK. Enhanced piezoelectric output voltage and Ohmic behavior in Cr-doped ZnO nanorods. Mater. Res. Bull. 2014;59:267–271.
40. Vojisavljević K, Ćepanović M, Srećković T, Grujić-Brojin M, Branković Z, Branković G. Structural characterization of mechanically milled ZnO: Influence of zirconia milling media. J. Phys. Condens. Matter. 2008;20: 475202.
41. Iqbal J, Jan T, Shafiq M, Arshad A, Ahmad N, Badshah S, Yu R. Synthesis as well as Raman and optical properties of Cu-doped ZnO nanorods prepared at low temperature. Ceram. Int. 2014;40:2091–2095.
42. Iqbal J, Safdar N, Jan T, Ismail M, Hussain SS, Mahmood A, Shahzad S, Mansoor Q. Facile synthesis as well as structural, raman, dielectric and antibacterial characteristics of Cu Doped ZnO nanoparticles. J. Mater. Sci. Technol. 2015;31:300–304.
43. Reddy AJ, Kokila MK, Nagabhushana H, Chakradhar RPS, Shivakumara C, Rao JL, Nagabhushana BM. Structural, optical and EPR studies on ZnO:Cu nanopowders prepared via low temperature solution combustion synthesis. J. Alloy Compd. 2011;509:5349–5355.
44. Suwanboon S, Amornpitoksuk P. Preparation and characterization of nanocrystalline La-doped ZnO powders through a mechanical milling and their opticalproperties. Ceram. Int. 2011;37:3515–3521.

45. Suwanboon S, Amornpitoksuk P, Bangrak P. Synthesis, characterization and optical properties of $Zn_{1-x}Ti_xO$ nanoparticles prepared via a high-energy ball milling technique. Ceram. Int. 2011;37:333–340.
46. Choudhury S, Sain S, Mandal MK, Pradhan SK, Meikap AK. Investigation of dielectric and electrical behaviour of nanocrystalline $Zn_{1-x}Mn_xO$ (x = 0 to 0.10) semiconductors synthesized by mechanical alloying, Phys. E Low-Dimensional Syst. Nanostructures. 2016;81:122–130.
47. Othman AA, Osman MA, Abd-Elrahim AG. The effect of milling time on structural, optical and photoluminescence properties of ZnO nanocrystals. Opt. -Int. J. Light Electron Opt. 2018;156:161–168.
48. Vijayaprasath G, Murugan R, Hayakawa Y, Ravi G. Optical and magnetic studies on Gd doped ZnO nanoparticles synthesized by co-precipitation method. J. Lumin. 2016;178:375–383.
49. Kumar S, Tiwari N, Jha SN, Chatterjee S, Bhattacharyya D, Ghosh AK. Structural and optical properties of sol–gel derived Cr-doped ZnO diluted magnetic semiconductor nanocrystals: an EXAFS study to relate the local structure. RSC Adv. 2016;6:107816–107828.
50. Mehedi Hassan M, Khan W, Azam A, Naqvi AH. Influence of Cr incorporation on structural, dielectric and optical properties of ZnO nanoparticles. J. Ind. Eng. Chem. 2015;21:283–291.
51. Sebayang K, Taslima S, Ginting M, Sebayang P, Bukit N. Cr-doped ZnO prepared by solid state reaction method. Chemistry and Materials Research. 2017;9:30–35.
52. Sartiman SS, Djaja NF, Saleh R. Chromium-doped ZnO nanoparticles synthesized by co-precipitation : chromium effects. Materials Sciences and Applications. 2013;2013:528–537.
53. Mote VD. Synthesis and characterization of Cr doped ZnO nanocrystals. World J. Condens. Matter Phys. 2012;2:208–211.
54. Zhang W, Liu Z, Liu Z, Zhao J. Effect of calcination temperature on the structural and optical properties of ZnO:Fe powders. Appl. Surf. Sci. 2012;258:6103–6106.
55. Bhargava R, Sharma PK, Kumar S, Pandey AC, Kumar N. Consequence of doping mediated strain and the activation energy on the structural and optical properties of ZnO:Cr nanoparticles. J. Solid State Chem. 2010;183:1400–1408.
56. Altintaş Yildirim O, Durucan C. Room temperature synthesis of Cu incorporated ZnO nanoparticles with room temperature ferromagnetic activity: Structural, optical and magnetic characterization. Ceram. Int. 2015;42:3229-3238.
57. Ozgür U, Alivov YI, Liu C, Teke A, Reshchikov MA, Doğan S, Avruti n V, Cho SJ, Morkç H. A comprehensive review of ZnO materials and devices. J. Appl. Phys. 2005;98:1–103.
58. Pandiyarajan T, Karthikeyan B. Cr doping induced structural, phonon and excitonic properties of ZnO nanoparticles. J. Nanoparticle Res. 2012;14: 647.
59. John R, Rajakumari R. Synthesis and characterization of rare earth ion doped nano ZnO synthesis and characterization of rare earth ion doped nano ZnO. Nano Micro Lett. 2016;2:65–72.

60. Das BK, Das T, Parashar K, Parashar SKS. Structural, bandgap tuning and electrical properties of Cu doped ZnO nanoparticles synthesized by mechanical alloying. J Mater Sci Mater Electron. 2017;28:1–8.
61. Yathisha RO, Nayaka YA, Vidyasagar CC. Microwave combustion synthesis of hexagonal prism shaped ZnO nanoparticles and effect of Cr on structural, optical and electrical properties of ZnO nanoparticles. Mater. Chem. Phys. 2016;181:167–175.
62. Vijayalakshmi K, Sivaraj D. Enhanced antibacterial activity of Cr doped ZnO nanorods synthesized using microwave processing. RSC Adv. 2015;5:68461–68469.
63. Kumaresan N, Ramamurthi K, Ramesh Babu R, Sethuraman K, Moorthy Babu S. Hydrothermally grown ZnO nanoparticles for effective photocatalytic activity. Appl. Surf. Sci. 2017; 418:138–146.
64. Azzez SA, Hassan Z, Hassan JJ, Mukhlif MS, Mahdi MS, Bououdina M. Effect of temperature on hydrothermally grown high-quality single-crystals Mg-doped ZnO nanorods for light-emitting diode application. J. Lumin. 2017; 192:634–643.
65. Shinde KP, Pawar RC, Sinha BB, Kim HS, Oh SS, Chung KC. Study of effect of planetary ball milling on ZnO nanopowder synthesized by co-precipitation. J. Alloys Compd. 2014; 617:404–407.
66. Kumar V, Kumari S, Kumar P, Kar M, Kumar L. Structural analysis by rietveld method and its correlation with optical propertis of nanocrystalline zinc oxide. Adv. Mater. Lett. 2015; 6:139–147.
67. Sinha AK, Gupta RK, Deb SK. A correlation between structural and optical properties of cobalt oxide nanoparticles for various annealing conditions. Appl. Phys. A. 2012; 108:607–613.
68. Das BK, Tanushree Das, Parashar K, Parashar SKS, Kumar R, Choudhary HK, Khopkar VB, Anupama AV, Sahoo B. Effect of Cr doping on structural, optical and dielectric properties of ZnO nanoceramics synthesized by mechanical alloying. Elect. Mater. Lett. 2020; 209:255–263.
69. Verma M, Dwivedi PK, Das B. Structure–property correlation of pure and Sn-doped ZnO nanocrystalline materials prepared by co-precipitation. J. Exp. Nanosci. 2015; 10:438–448.
70. Kadam AN, Kim TG, Shin DS, Garadkar KM, Park J. Morphological evolution of Cu doped ZnO for enhancement of photocatalytic activity. J. Alloys Compd. 2017; 710:102–113.
71. Ping C, Yue B. Structure and optical properties of electrodeposited Nd-doped ZnO thin films. Rare Met. Mater. Eng. 2016; 45:1419–1422.

Biography of author(s)

Bikram Keshari Das
Nano Innovation Laboratory,School of IKST, Kalinga Institute of Social Sciences (KISS) Deemed to be University, Bhubaneswar-751024, Odisha, India.

Research and Academic Experience: He has completed Post-Graduation from North Orissa University, Baripada and Ph.D from KIIT University, India. His research is on Nano Materials synthesis, Characterization and their applications. He has more than 17 years of teaching experience and 10 years of research experience. Presently he is working as an Assistant Professor in KISS University, Bhubaneswar. Before joining KISS University he was working as an Assistant Professor in Orissa Engineering College, Bhubaneswar.

Research Area: Nano Materials, Nano ceramics, Electronic materials, piezoelectric materials etc.

Number of Published Papers: He has published many research papers in international journals.

Other Remarkable Point(s): He is the member of one scientific body. He has successfully organized many national and international conferences. He has guided many M.Sc students. Dr. Das has one on-going DST sponsor project.

Tanushree Das
Nano Innovation Laboratory, School of IKST, Kalinga Institute of Social Sciences (KISS) Deemed to be University, Bhubaneswar-751024, Odisha, India.

Research and Academic Experience: She obtained her M.Sc. (Chemistry), M.Phil degree from North Orissa University, Baripada and Ph.D degree from KIIT University, Bhubaneswar, India in the year 2018. She has been working in KISS University since 2018. She has been actively engaged in teaching and research.

Research Area: Her basic area of research is synthesis and characterization of Nanomaterials for different applications like photocatalytic, thermistor, varistor, sensor etc.

Number of Published Papers: She has published many research papers in different international journals.

Other Remarkable Point(s): She is handling one SERB sponsor project, Govt. of India as principal investigator and guided many M.Sc students.

Dipteerekha Das
Nano Innovation Laboratory, School of IKST, Kalinga Institute of Social Sciences (KISS) Deemed to be University, Bhubaneswar-751024, Odisha, India.

Research and Academic Experience: She has completed her M.Sc. in Chemistry and M.Phil degree from North Orissa University, Baripada, India in the year 2012. She was working as a lecturer in Chemistry for last six years. Presently she is working as a Research Fellow in KISS University since 2020.

Research Area: Her basic area of research is synthesis and characterization of Nanomaterials, Electronics materials and and their application as sensor.

Number of Published Papers: She has published three research papers in different international journals.

Peer-Review History: During review of this manuscript, double blind peer-review policy has been followed. Author(s) of this manuscript received review comments from a minimum of two peer-reviewers. Author(s) submitted revised manuscript as per the comments of the peer-reviewers. As per the comments of the peer-reviewers and depending on the quality of the revised manuscript, the Book editor approved the revised manuscript for final publication.